Hindawi
Journal of Nanomaterials
Volume 2018, Article ID 3738106, 14 pages
https://doi.org/10.1155/2018/3738106

Research Article

Microstructural Analysis and Magnetic Characterization of Native and Magnetically Modified Montmorillonite and Vermiculite

Yvonna Jiraskova,[1] **Jiri Bursik**,[1] **Jana Seidlerova**,[2] **Katerina Mamulova Kutlakova**,[2] **Ivo Safarik**,[3,4] **Mirka Safarikova**,[3] **Kristyna Pospiskova**,[4] **and Ondrej Zivotsky**[5,6]

[1]*CEITEC IPM, Institute of Physics of Materials, Academy of Sciences of the Czech Republic, Zizkova 22, 616 00 Brno, Czech Republic*
[2]*Nanotechnology Centre, VSB–Technical University of Ostrava, 17. listopadu 15/2172, 708 33 Ostrava-Poruba, Czech Republic*
[3]*Department of Nanobiotechnology, Biology Centre, ISB, CAS, Na Sadkach 7, 370 05 Ceske Budejovice, Czech Republic*
[4]*Regional Centre of Advanced Technologies and Materials, Palacky University, Slechtitelu 27, 783 71 Olomouc, Czech Republic*
[5]*Department of Physics, VSB–Technical University of Ostrava, 17. listopadu 15/2172, 708 33 Ostrava-Poruba, Czech Republic*
[6]*Boris Yeltzin Ural Federal University, 620002 Ekaterinburg, Russia*

Correspondence should be addressed to Yvonna Jiraskova; jirasko@ipm.cz

Received 16 May 2018; Revised 3 August 2018; Accepted 19 August 2018; Published 10 October 2018

Academic Editor: Luciano Carlos

Two clay minerals of the similar 2 : 1 layer structure and chemical composition, vermiculite and montmorillonite, were studied using a wide spectrum of experimental methods in their original states and the magnetically modified states after mixing with microwave-synthesized iron oxide particles. This magnetic modification led to different microstructural morphology influencing magnetic behaviour at room and more pronounced at low temperatures.

1. Introduction

The clay minerals, defined as a class of hydrated phyllosilicates [1], are the primary products of chemical weathering and the more abundant constituents of sedimentary rocks. From this viewpoint, their investigation is of high importance as it follows from many studies over the world, e.g., [2–4].

The basic unit of phyllosilicates (including clay minerals) is based on interconnected rings of SiO_4^{4-} tetrahedron that extend in infinite sheets [5]. Three apical oxygen atoms from each tetrahedron are shared with other tetrahedron, and the fourth apical oxygen points vertically upon the sheet. In such a way, a basic structural unit $Si_2O_5^{2-}$ is formed, and in an ideal case, the sheet yields a hexagonal symmetry, see Figure 1. Nevertheless, the tetrahedral position can be occupied also by Al atoms, and in such a way, the tetrahedral sheet is deformed, and its symmetry is lower than hexagonal.

An integral part forms the sheets of octahedrons $X(O, OH)_6$ which share not only vertexes but also a half of edges. Octahedrons are tagged together by the octahedron plane perpendicularly to [001] so that three anions (O^- or OH^-) form a lower layer, three anions are in the upper layer and in between the octahedral cations (X), mostly Al, Fe, and Mg, are present. The occupation of the structural positions in the octahedral sheet generates trioctahedral sheet silicates where each O or OH is surrounded by 3 divalent cations, like Fe(II) or Mg(II), and dioctahedral sheet silicates where each O or OH ion is surrounded by 2 trivalent cations, mostly Al(III) [5].

The individual sheets can be variously connected. If the tetrahedral and octahedral sheets have one shared plane of oxygen atoms, the phyllosilicates are of type 1 : 1 (layers t-o). The type 2 : 1 (layers t-o-t) means that one octahedral sheet shares two tetrahedral sheets of opposite polarity. Then each tetrahedral sheet joins the octahedral sheet from one side with its apical oxygen atoms. A space

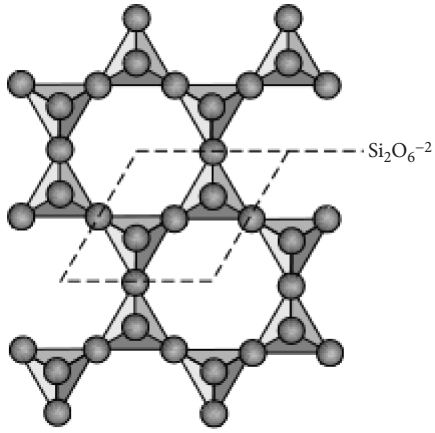

Figure 1: The basic structural unit of phyllosilicates.

between layers is denoted as interlayer, and one layer with interlayer forms a basic structural unit of phyllosilicates. The layers can be combined regularly or irregularly and can be electrically neutral or they can carry a certain negative charge due to substitutions. A charge size determines a mechanism of a mutual bond between layers in a structure [5]. Clay minerals are classified pursuant to several mentioned criteria: (i) layer type (1 : 1, 2 : 1), (ii) type of interlayer (water or interlayer cation), (iii) charge of layer, (iv) type of octahedral sheets (di- or trioctahedral), and (v) chemical composition. In accordance with these criteria, they are divided into a few groups [1, 6]. The clay minerals chosen for the present studies were montmorillonite from the group of smectites and vermiculite from the group of vermiculites.

Montmorillonite (Mt) is a member of the smectite group containing the layer of the 2 : 1 type. It means that it has two tetrahedral sheets of silica SiO_4 sandwiching a central octahedral sheet of one AlO_6 (Figure 2(a), [7]). The particles are plate-shaped with an average diameter lower than 2 μm and a thickness of about 10 nm. Water molecules and cations occupy the space between the 2 : 1 layers. Generally, the crystalochemical formula is $(Si_4)^{IV}(Al_2 - yMg_y)^{VI}O_{10}(OH)_2xX^+ \cdot nH_2O$, where X represents mono- (e.g., Na(I), K(I)) or divalent interlayer cations (Ca(II), Fe(II)). These mono- or divalent cations balance the negative charge of montmorillonite layers [8]. Essentially, the clay mineral can be modified in two ways: in the interlayer space in pursuance of swelling and cation exchange and on the surface due to an adsorption process.

Vermiculite (Ver) is also a layered clay mineral composed of two sheets of SiO_4 [9]; tetrahedra coupled symmetrically to another sheet of MgO_6^{4-} octahedral in a tetrahedral-octahedral-tetrahedral layer lattice (Figure 2(b), [7]). The basic characteristics can be found in [10]. The theoretical formula is $(X_v \cdot nH_2O)(R_z^{2+}R_y^{3+})(Al, Fe^{3+})(Si_4O_{10})(OH)_2$, where X represents mono- or divalent cations located primarily in the interlayer. The natural vermiculite contains usually the hydrated Mg(II) cations located at the surface. They balance the negative charge of the SiO_4^- anions. In accordance with a structural analysis of Shirozu and Bailey [11], the Mg interlayer is octahedral coordinated with water molecules forming a mono-octahedral sheet.

The abovementioned clay minerals are widely used in the building and foundry industries, as a part of the thin layers and composites in modern technologies. They are also used in acoustics and in agriculture as fireproof insulators, fertilizer carriers, etc. [1]. For their high specific surface area, chemical and mechanical stabilities, variety of structural and surface properties, and high values of cation exchange capacities, they are an excellent group of adsorbents [12, 13]. Montmorillonite and vermiculite are used as effective sorbents for removing toxic ions [14–18], toxic molecules from waste water [19–21], dyes [22–25], or other compounds [26, 27].

In the last years, new materials are designed to improve sorption efficiency, decrease the price of purification technology, and enhance the functionality of a material. In order to improve the sorption properties of clay minerals, different acid activation and other chemical procedure modification were developed [28–31]. Most of the papers are devoted to the improvements of clay minerals from the viewpoint of their applications [32, 33]. Clay minerals modified by metal oxides in their interlayer space are known as pillared clays. The oxide particles act as pillars and keep silicate layers apart and form two-dimensional molecular sieves. Compared to original clay minerals, they have a higher fraction of the surface area.

In present study, the main attention is devoted to analysis of the complex structural and magnetic properties of the magnetically modified montmorillonite (MMt) and vermiculite (MVer) using the iron oxide particles and of the original, unmodified clay minerals (Mt, Ver). The structural properties, morphology and chemical composition, are determined by X-ray fluorescence spectroscopy (XRFS), scanning electron microscopy (SEM), transmission electron microscopy (TEM), and X-ray diffraction (XRD). The macro- and micromagnetic characterizations of samples are achieved by the magnetic and Mössbauer measurements at room and elevated temperatures completed by the low-temperature measurements.

2. Experiment

2.1. Sample Preparation. Two different types of clay minerals were used in present studies: montmorillonite (Mt) and vermiculite (Ver). Montmorillonite consists of a double aluminium and magnesium silicates. It was obtained from a product of the Beaufour Ipsen Industrie (France) which is used in medicine as diosmecticum containing besides montmorillonite also glucose, saccharine, and vanilla. These three components had to be removed by water leaching to obtain pure montmorillonite. Vermiculite was obtained from the Paraiba region of Brazil occurring in Santa Luzia [34].

The newly developed, relatively simple, procedure was applied for magnetic modification of both studied clay

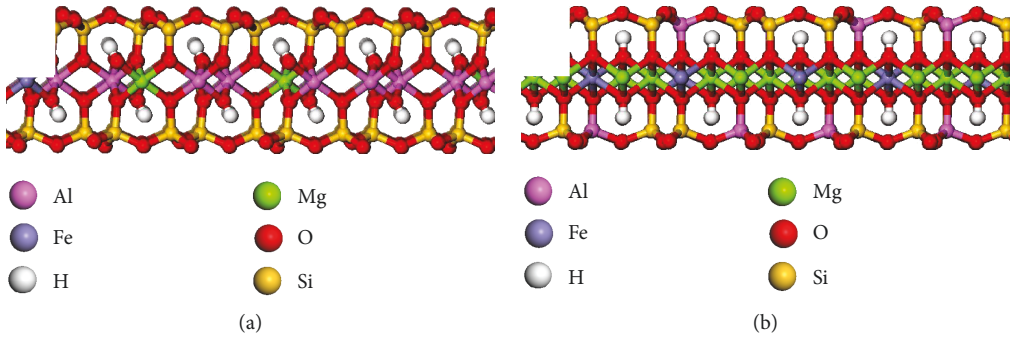

Figure 2: Chemical structure of montmorillonite (a) and vermiculite (b) [7].

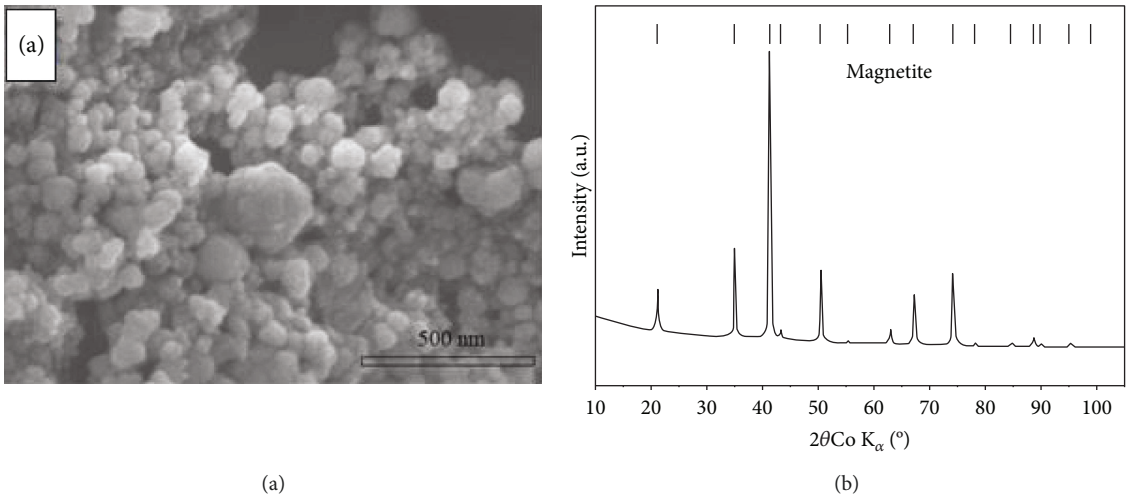

Figure 3: SEM micrograph (a) and X-ray powder diffraction pattern (b) of iron oxide nanoparticles prepared by microwave-assisted synthesis.

minerals. Initially, the magnetic iron oxide nanoparticles were prepared from a single Fe2+ salt—ferrous sulfate, employing a microwave irradiation according to the following procedure: 2 g $FeSO_4 \cdot 7H_2O$ was dissolved in 100 ml of water in an 800 ml beaker. Subsequently, NaOH solution (1 mol l^{-1}) was slowly added under stirring whereas the iron hydroxide precipitates were formed by monitoring pH. At pH 11–12, the beaker with suspension was filled with water to amount of 250 ml and inserted into a standard domestic microwave oven (700 W, 2.45 GHz) for 10 min. This resulted in the suspension containing magnetic iron oxide particles which were repeatedly washed with water to remove completely the rest of NaOH [35, 36]. The morphology of the final iron oxide powder is shown in Figure 3(a). An analysis of particle dimensions from the SEM images has yielded their mean size ranging between 25 nm and 100 nm. Sporadically, particles below 25 nm were also present. The analysis of the X-ray pattern in Figure 3(b) yielded the presence of pure magnetite with the lattice parameter $a = 0.8396(3)$ nm, in good agreement with literature data, e.g., [37]. The mean crystallite size was determined to be 43 nm.

In the next step, 10 ml suspension of iron oxide particles and water in ratio 1 : 4 (v/v; magnetic particles sedimented overnight at 1 g) was mixed with 5 g of dried clay mineral Mt and/or Ver and stirred using a laboratory spoon as long as a homogeneous distribution of iron oxide particles in the clay mineral was obtained. Finally, the mixture was dried completely at 40°C.

2.2. Experimental Methods

2.2.1. Scanning Electron Microscopy (SEM). The morphology of iron oxide nanoparticles was analyzed by SEM 120 Hitachi SU6600 (Hitachi, Tokyo, Japan) with accelerating voltage 5 kV and by TESCAN LYRA 3XMU FEG/SEM scanning electron microscope working at accelerating voltage of 20 kV. The second microscope equipped with an XMax80 Oxford Instrument detector for EDX was used for the chemical composition of powdered samples pressed into a small disc of 3 mm in diameter.

2.2.2. X-Ray Fluorescence Spectroscopy (XRFS). The XRFS was performed using an energy dispersive spectrometer

equipped by Pd X-ray tube with Be window, 50 W/50 kV, targets HOPG, Mo, Al_2O_3, Xflash drift chamber, Si detector with Pelletier's cooling and resolution of 170 eV on line Mn Kα at 10000 pulse/s (XEPO.S, Spectro AI, Germany).

2.2.3. Transmission Electron Microscopy (TEM). A Jeol 2010 HC (resolution limit—0.19 nm) with a LaB_6 crystal cathode operating at 200 kV was used to study the microstructure of powders. Samples for TEM study were treated ultrasonically in an ethanol bath for 5 minutes and then placed on holey carbon copper grids for observations in an electron microscope.

2.2.4. X-Ray Powder Diffraction (XRD). X-ray powder diffraction measurements were done at room temperature (RT) using X'PERT PRO diffractometer by Panalytical. The samples were measured in a form of a small disc about 2 mm in diameter and approximately 500 μm thick prepared by powder pressing and used subsequently for thermomagnetic measurements. The patterns were taken in a reflection mode using CoKα irradiation ($\lambda = 0.1789$ nm), Bragg-Brentano geometry, 2θ range 10°–100°, with 0.008° step and time per step 250 s.

2.2.5. Mössbauer Spectrometry. Mössbauer measurements were carried out at room and low (7 K) temperatures in standard transmission geometry using a ^{57}Co(Rh) source. The calibration of the velocity scale was performed with α-Fe, and the isomer shifts are given with respect to the RT Mössbauer spectrum of α-Fe. All spectra were evaluated within the transmission integral approach using the program CONFIT [38]. In the measured Mössbauer spectrum, the ferromagnetic (fm) phases are represented by sextuplets while the paramagnetic (pm) phase by singlets and/or doublets of Lorentzian lines. The phases can be characterized by either one or more subspectra depending on the atom ordering in the structure. All subspectra are characterized by discrete values of hyperfine parameters: isomer shift (δ), quadrupole splitting (ΔEQ) for pm, fm phase(s), and hyperfine induction (B) for fm phase(s). A weakly resolved atom ordering and/or highly defected region are represented by a distribution of hyperfine induction. The relative representation of phases is denoted by A.

2.2.6. Magnetic Measurements. The magnetic properties were studied using the vibration sample magnetometers (VSM) Microsense EV9 and Physical Property Measurement System (PPMS) Quantum Design Inc. Hysteresis curves describing the dependence of the mass magnetization on the applied magnetic field H were measured at room temperature (RT≈300 K) in an external field up to ±1600 kA/m (2 T) and at low temperature (LT≈2 K) up to ±4000 kA/m (5 T). The magnetic parameters, mass magnetization at 2 T and 5 T, remnant magnetization, and coercivity, were determined from the hysteresis curves with an accuracy ±1% [39]. To analyze the magnetic interactions among particles, the Henkel plot was constructed. It represents a relation between the initial (virgin) curve, $M_{\text{vir}}(H)$, and magnetizations at increasing (M_{UP}) and decreasing (M_{DOWN}) positive magnetic fields [40]:

$$\Delta M(H) = M_{\text{VIR}}(H) - \frac{M_{\text{UP}}(H) + M_{\text{DOWN}}(H)}{2}. \quad (1)$$

The zero-field-cooled (ZFC) and field-cooled (FC) curves were measured between 2 K and 300 K in a magnetic field of 8 kA/m. The thermomagnetic curves (TMC) representing magnetic behaviour of samples at elevated temperatures were obtained in an external magnetic field of 8 kA/m, temperature increase of 4 K/min up to 1073 K, and vacuum to prevent oxidation. The transition from the magnetic to nonmagnetic state is characterized by a decrease in magnetization to zero value at Curie temperature. It was determined from the TMC with accuracy of about ±5 K.

3. Results and Discussion

3.1. Chemical Composition and Morphology. The results of chemical analysis of the original (Mt, Ver) and magnetically modified (MMt, MVer) samples using XRFS and EDX are summarized in Table 1. An increase in content of the iron oxides after magnetic modification is evident at both samples. Besides Fe_2O_3, a small amount of wüstite $Fe_{1-x}O$ was detected. A total content of iron oxides 8.38 wt% was slightly higher in vermiculite (MVer) compared to 5.62 wt% in montmorillonite (MMt).

SEM observations of both Mt and Ver samples have yielded similar morphology as seen in Figure 4. To obtain information about the chemical homogeneity, the Mt sample was chosen as an example for the local-dot and large area EDX chemical analyses summarized in Figure 5. The table corresponding to SEM image demonstrates that both large area (a) and local-dot analyse (b) show a dispersion smaller than 1% and thereby prove a high homogeneity of powder up to 1 micrometer level. The EDX analyses in Figure 5 were quantified and normalized without oxygen due to generally lower sensitivity of EDX for light elements. The results of elements were further recalculated with respect to oxygen stoichiometry of constituent phases, and the obtained values are given in Table 1 where they are compared with normalized data obtained by chemical analysis and recalculated without loss on ignition (LOI). A good agreement in obtained data is seen for all samples.

The more detail morphology of the vermiculite and montmorillonite samples in their original (Ver, Mt) and modified (MVer, MMt) states is seen in the TEM micrographs in Figure 6. They document that the submicron iron oxide nanoparticles occur at the surface and intergrain of the MVer and MMt samples and that their size is surprisingly larger at the MVer sample though the preparation procedure was the same for both clay minerals. This corresponds with a difference in XRD patterns of the magnetically modified samples in the next subsection.

Table 1: Chemical composition in wt% of the montmorillonite and vermiculite in their original states (Mt, Ver) and after the magnetic modification (MMt, MVer). LOI is loss on ignition; Mt_n, MMt_n,Ver_n, and $MVer_n$ denote normalized contents without LOI. Mt_{EDX}, MMt_{EDX}, Ver_{EDX}, and $MVer_{EDX}$ are the values obtained by EDX analysis and recalculated with respect to oxygen.

	Mt	Mt_n	Mt_{EDX}	MMt	MMt_n	MMt_{EDX}	Ver	Ver_n	Ver_{EDX}	MVer	$MVer_n$	$MVer_{EDX}$
Al_2O_3	14.4 ± 1.1	17.28	17.28	14.1 ± 1.2	18.23	16.68	10.5 ± 0.8	12.62	12.60	10.4 ± 0.8	12.32	14.18
SiO_2	55.5 ± 2.3	70.28	73.56	54.1 ± 2.2	70.28	69.85	39.6 ± 1.6	67.46	51.63	39.2 ± 1.6	46.42	51.37
TiO_2	0.17 ± 0.02	0.22	0.23	0.17 ± 0.02	0.22	0.25	1.03 ± 0.12	1.24	1.40	1.02 ± 0.12	1.21	0.34
Na_2O	0.20 ± 0.02	0.25	0.26	0.20 ± 0.02	0.25	0.16	0.50 ± 0.05	0.60	0.54	0.50 ± 0.05	0.59	0.07
K_2O	0.16 ± 0.0	0.20	0.14	0.16 ± 0.01	0.20	0.16	2.20 ± 0.14	2.64	3.74	2.18 ± 0.03	2.58	0.03
MgO	4.13 ± 0.25	5.23	4.54	4.03 ± 0.25	5.03	4.06	21.1 ± 1.28	25.37	18.28	20.9 ± 1.25	24.75	22.72
CaO	1.85 ± 0.12	2.34	2.14	1.81 ± 0.11	2.26	2.25	1.88 ± 0.13	2.26	2.20	1.86 ± 0.12	2.20	0.17
Fe_2O_3	2.56 ± 0.10	3.24	1.87	4.69 ± 0.09	3.24	6.58	6.37 ± 0.25	7.66	9.61	7.54 ± 0.15	8.93	11.11
FeO	—	—		0.93 ± 0.08	1.16		—	—		0.84 ± 0.08	0.99	
LOI	21.30 ± 0.30	—	—	20.30 ± 0.40	—	—	19.44 ± 0.02	—	—	19.60 ± 0.40	—	—

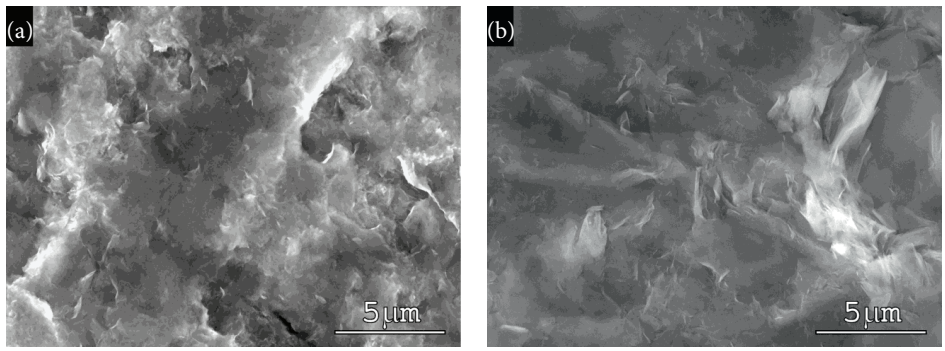

(a) (b)

Figure 4: Morphology of the original (a) montmorillonite (Mt) and (b) vermicullite (Ver) samples obtained by SEM in the secondary electron mode.

3.2. X-Ray Diffraction. The X-ray diffraction patterns in Figure 7 represent the vermiculite (a) and montmorillonite (b) in their original (Ver, Mt) and magnetically modified (MVer, MMt) states. The diffraction patterns of both clay minerals are highly sensitive to chemical composition and to a strong texture consequently the layered nature as it follow from more detail studies of the vermiculite and/or montmorillonite taken from various geographic regions (e.g., [41–43]). The analysis of both magnetically modified samples did not yield any input of iron oxide nanoparticles into interlayers. The complicated composition of both clay samples was a reason why more detailed analysis of all patterns has remained out of the present study. The X-ray patterns in Figure 7 have only to document a difference between the original and the magnetically modified states. This difference is remarkably higher in the low-angle region for 2θ between 10° and 40° (upper panels), namely, at vermiculite. The outstanding peaks in both vermiculite samples (Ver, MVer) at $2\theta = 21.79°–29.07°–36.48°–44.27°–52.07°$ yield nearly the same positions. At present, it can be only speculated that the magnetic modification did not affect the structure of the sample. From the structural viewpoint, more detailed studies of both modified clay minerals should be done.

3.3. Mössbauer Spectrometry. The Mössbauer spectra of the original (Mt, Ver) and magnetically modified (MMt, MVer) montmorillonite and vermiculite samples recorded at room and low (7 K) temperatures are depicted in Figure 8. While the X-ray diffraction yields information on the major minerals in clays, Mössbauer spectroscopy looks selectively at the iron-containing compounds that are often difficult to detect by X-ray diffraction due to their low concentration, small particle size, or poor crystallinity. Nevertheless, also a unique interpretation of Mössbauer spectra can be sometimes difficult or impossible, either because the spectrum cannot be decomposed in a unique shape into individual components, or because different iron-based components have very similar Mössbauer patterns. Sometimes, it is helpful to supplement the measurements at ambient temperature by measurements at liquid nitrogen or helium temperatures.

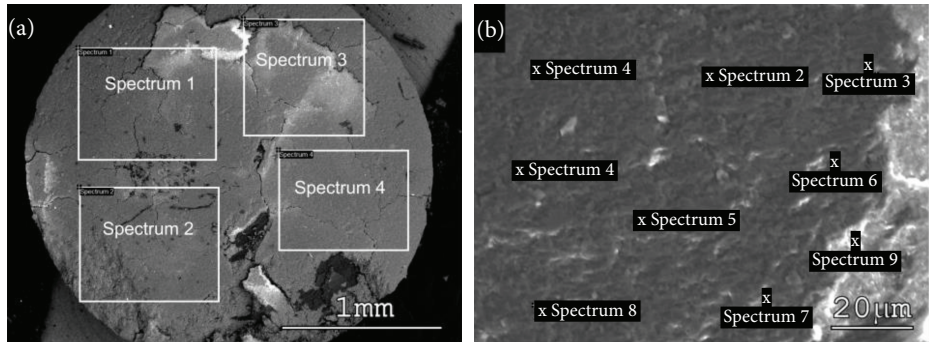

	Spect.	Na	Mg	Al	Si	K	Ca	Ti	Fe
(a)	1	0.48	5.54	18.36	69.50	0.17	3.02	0.20	2.72
	2	0.34	5.39	18.05	68.87	0.19	3.76	0.34	3.06
	3	0.38	5.62	18.83	69.90	0.16	2.75	0.30	2.07
	4	0.32	5.43	18.32	69.08	0.34	3.14	0.39	2.97
	Mean	0.38	5.49	18.39	69.34	0.22	3.17	0.31	2.71
	Stdv.	0.07	0.11	0.32	0.46	0.09	0.43	0.08	0.42
(b)	1	0.44	6.23	18.59	71.09	0.01	2.46	0	1.21
	2	0.33	5.97	19.14	69.72	0.25	2.09	0.64	1.86
	3	0.23	6.97	19.09	69.71	0.24	2.37	0.02	1.36
	4	0.38	6.64	18.23	70.99	0.08	2.43	0.11	1.14
	5	0.39	5.50	20.03	70. 48	0.13	2.11	0.04	1.32
	6	0.48	6.55	18.30	70.41	0.16	2.47	0.11	1.52
	7	0.22	5.65	19.48	70.00	0.36	2.37	0.24	1.67
	8	0.45	5.49	20.04	70.59	0	2.17	0.10	1.18
	9	0.62	6.03	18.11	70.91	0.24	2.37	0.28	1.45
	Mean	0.39	6.12	19.00	70.43	0.16	2.32	0.17	1.41
	Stdv.	0.12	0.53	0.74	0.53	0.12	0.15	0.20	0.24

Figure 5: SEM micrographs of sample Mt with marked large area (a) and point (b) EDX analyses.

Iron may be present in both minerals as Fe(II) and Fe(III) and on positions with a tetrahedral or octahedral oxygen environment. They can be distinguished by hyperfine parameters, namely, isomer shift and quadrupole splitting.

The Mössbauer spectra for the Ver sample in its original state collected at 295 K and at 7 K are shown in Figure 8(a)—upper panel. The low-temperature spectrum yields a weak magnetically broadened six-line component with relative area of 3.6% pointed up in black color in the same way as in other spectra. Its hyperfine induction 51 T is slightly lower as obtained by other authors [40, 43]. The small relative area as well as isomer shift ($\delta = 0.37$ mm/s) and quadrupole splitting ($\Delta EQ = -0.45$ mm/s) make difficult an assignment to a specific oxide or oxyhydroxide. The magnetic modification of vermiculite (MVer) has contributed to an increase in relative area of magnetic component to 9.8% at RT and to 18.2% at 7 K. The hyperfine parameters obtained by analysis of the RT Mössbauer spectrum, $B = 46.82(33)$ T, $\delta = 0.55(5)$ mm/s, $\Delta EQ = -0.26(10)$ mm/s, and of the low-temperature spectrum, $B = 51.70(16)$ T, $\delta = 0.42(2)$ mm/s, $\Delta EQ = -0.06(4)$ mm/s, reflect rather a complex iron (oxide, hydroxide, and oxyhydroxide) due to the presence of Al, Fe, and Ti cations and the anionic part either of oxygen (–O) and of the hydroxyl group (–OH or –OOH). These results are supported also by the fact that the low-temperature spectrum consists of not only single sextuplets but also the hyperfine induction representing the mean value of the Gaussian hyperfine distribution with a width of 4.9(6) T. A more detail assignment to a certain component is also difficult because of variations in crystallinity.

The dominant paramagnetic fraction of all spectra has been fitted by four symmetric doublets whose parameters are listed in Table 2 for vermiculite samples and both temperatures. The doublets with isomer shift of ca. 1 mm/s can be assigned to Fe(II) ions and with smaller one around to Fe(III) in agreement with other authors [44–46].

The amount of iron-based compounds is in original montmorillonite (Mt) sample low as it results from the chemical analysis. The Mössbauer spectra are presented in Figure 8(b), upper panel. The parameters of doublets are summarized for both RT and low temperature in Table 3. The magnetic six-line components are seen in

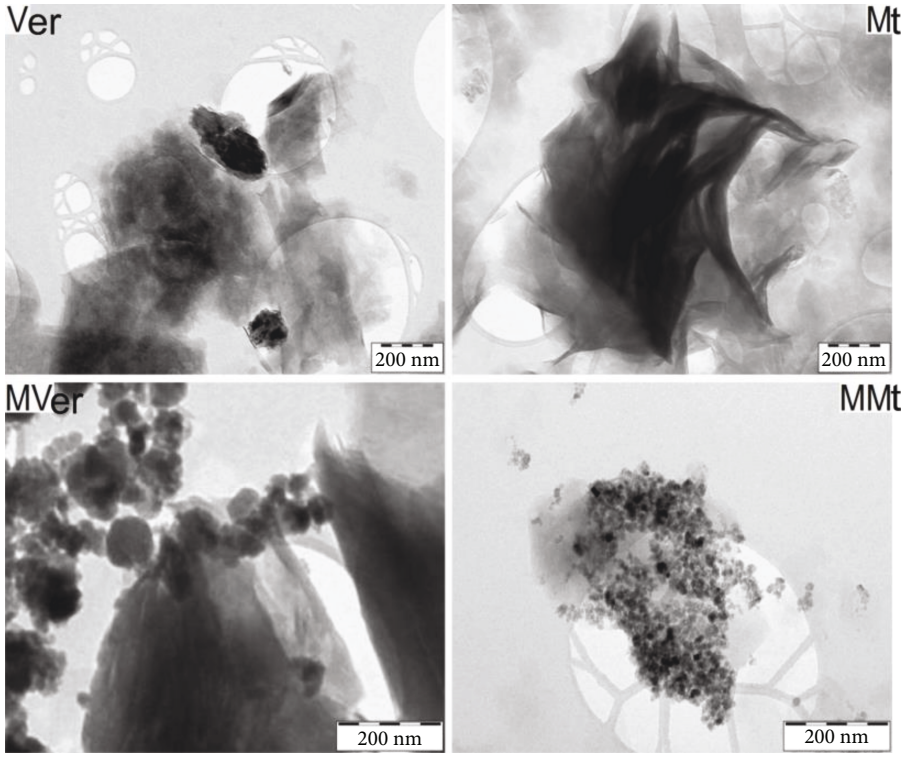

Figure 6: TEM micrographs of the original (Ver, Mt) and magnetically modified (MVer, MMt) clay minerals.

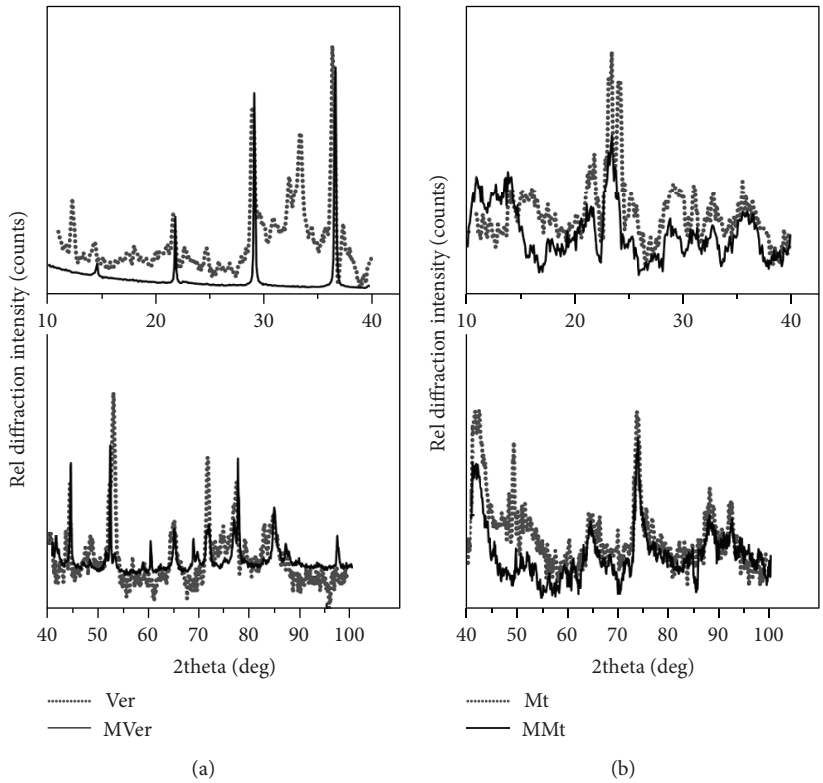

Figure 7: Room temperature reflection X-ray powder diffraction patterns of vermiculite (a) and montmorillonite (b) in the original (Ver, Mt) and magnetically modified (MVer, MMt) states.

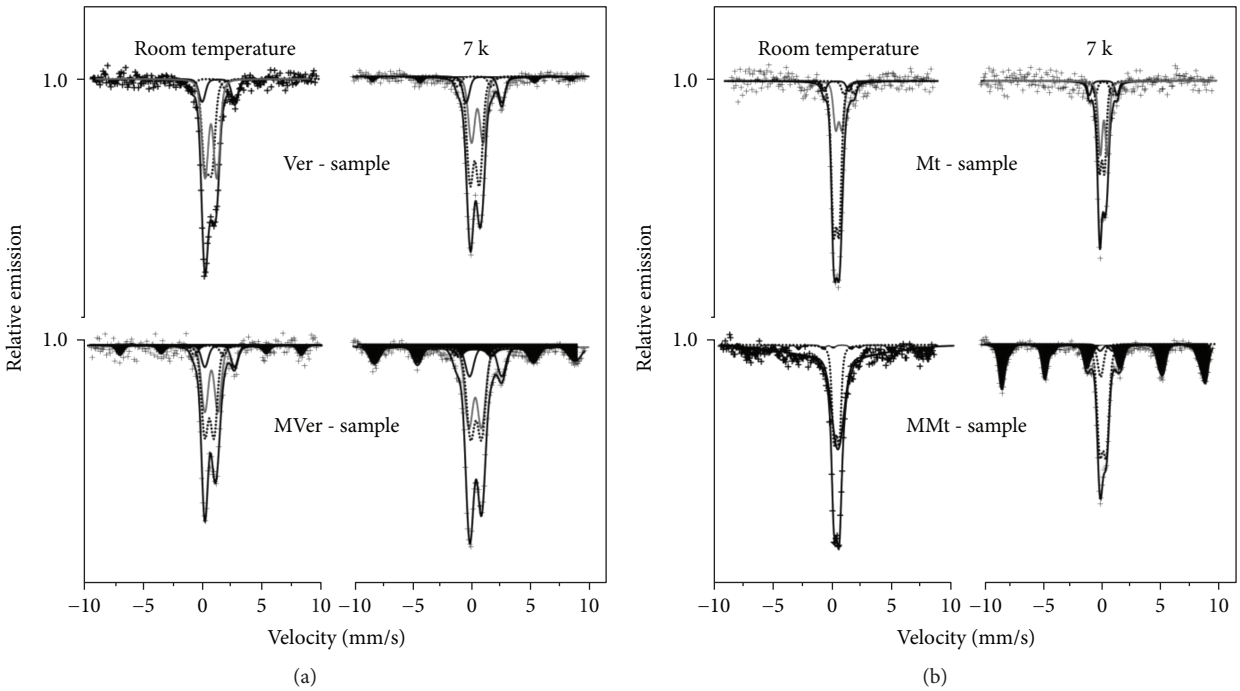

Figure 8: Mössbauer spectra of the original (Ver, Mt) and magnetically modified (MVer, MMt) vermiculite (a) and montmorillonite (b) samples measured at room and low temperatures.

Table 2: Mössbauer parameters of paramagnetic fraction in the vermiculite samples; original (Ver) and magnetically modified (MVer) state; T (K): temperature of measurement.

T (K)	295		7	
	Ver	MVer	Ver	MVer
δ_1 (mm/s)	0.44 (1)	0.48 (3)	0.61 (2)	0.43 (3)
δ_2 (mm/s)	0.24 (1)	0.32 (2)	0.39 (1)	0.48 (3)
δ_3 (mm/s)	0.22 (1)	0.28 (7)	0.39 (4)	0.30 (5)
δ_4 (mm/s)	1.07 (4)	1.17 (2)	1.16 (2)	1.37 (2)
ΔEQ_1 (mm/s)	0.97 (2)	1.09 (6)	0.97 (4)	1.05 (7)
ΔEQ_2 (mm/s)	0.57 (2)	0.76 (4)	0.76 (2)	0.95 (5)
ΔEQ_3 (mm/s)	2.74 (12)	2.40 (16)	2.81 (8)	2.92 (10)
ΔEQ_4 (mm/s)	2.71 (9)	2.46 (4)	2.96 (4)	2.55 (4)

Table 3: Mössbauer parameters of paramagnetic fraction in the montmorillonite samples; original (Mt) and magnetically modified (MMt) state; T (K): temperature of measurement.

T (K)	295		7	
	Mt	MMt	Mt	MMt
δ_1 (mm/s)	0.41 (6)	0.22 (1)	0.48 (3)	0.42 (1)
δ_2 (mm/s)	0.20 (3)	0.31 (1)	0.32 (3)	0.22 (1)
δ_3 (mm/s)	1.26 (3)	—	0.46 (4)	0.67 (1)
δ_4 (mm/s)	0.22 (6)	—	0.42 (4)	—
ΔEQ_1 (mm/s)	0.52 (7)	0.42 (1)	0.58 (5)	0.54 (1)
ΔEQ_2 (mm/s)	0.46 (1)	0.04 (1)	0.42 (3)	0.00 (1)
ΔEQ_3 (mm/s)	0.84 (10)	—	1.36 (13)	1.02 (1)
ΔEQ_4 (mm/s)	2.06 (14)	—	2.30 (7)	—

the magnetically modified montmorillonite (MMt) occupying relative area of about 11% at RT and 51% at low temperature. The hyperfine parameters obtained for the MMt sample at RT, $B = 44.9$ T, $\delta = 0.46$ mm/s, $\Delta EQ = -0.02$ mm/s, and at 7 K, $B = 51.5$ T, $\delta = 0.45$ mm/s, $\Delta EQ = -0.06$ mm/s, are typical for nanocrystalline γ-Fe_2O_3 particles [47–49]. Similar to the MVer sample, the assignment of obtained values of the hyperfine parameters accurately to the specific iron oxide or oxyhydroxide is again difficult and not unique.

3.4. Magnetic Properties. The RT hysteresis curves, Henkel plots, and corresponding magnetic parameters of samples are depicted in Figure 9 and in Table 4, respectively. Montmorillonite (Mt) and vermiculite (Ver) in the original state own the coercive field of about 2.44 kA/m and 0.945 kA/m and nearly the same low values of remanent magnetization. The magnetization at 2 T is higher at the Ver sample (0.275 Am^2kg^{-1}) compared to 0.057 Am^2kg^{-1} at the Mt sample that corresponds with higher iron oxide compounds found out by the chemical analysis (see Table 1). The magnetic field of 1.6 MA/m (2 T) is sufficient to saturate only the montmorillonite while at the vermiculite, the magnetization increase linearly above 100 kA/m of applied field and a substantial field is required to saturate it entirely. The magnetic modification leads to visible change in magnetization curves of both samples that are nearly saturated above 800 kA/m. The modified montmorillonite (MMt) exhibits higher saturation magnetization and markedly lower values of the remanent magnetization and coercivity (Table 4). It relates with higher relative area of the ferromagnetic

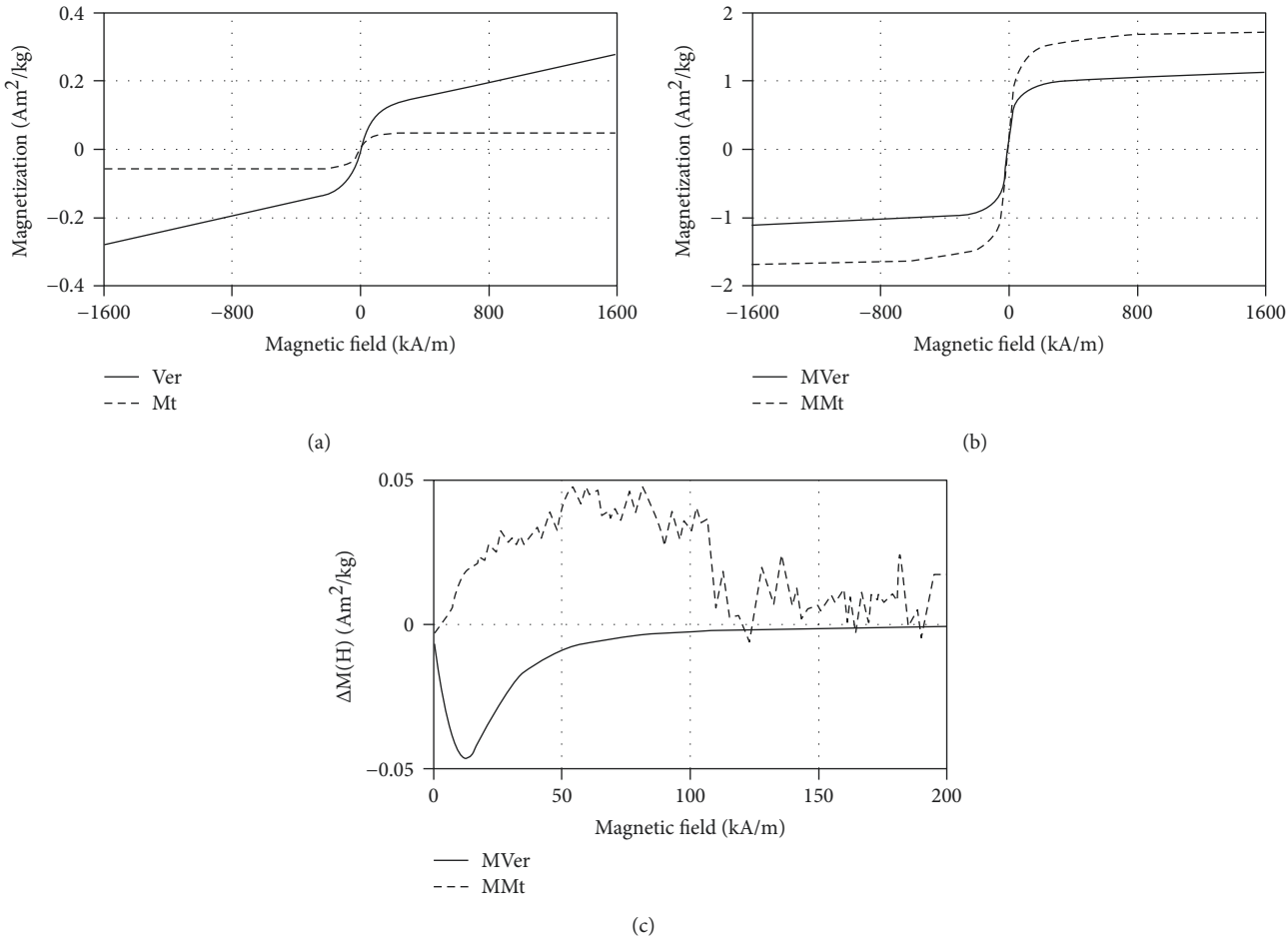

Figure 9: Room temperature magnetization curves of original samples (a), magnetically modified samples (b), and Henkel plots of MVer and MMt samples (c).

Table 4: Room temperature (RT≈300 K) and low-temperature (LT≈2 K) magnetic parameters of the original (Mt, Ver) and magnetically modified (MVer, MMt) vermiculite and montmorillonite samples; M: magnetization; M_r: remanent magnetization; H_c: coercivity.

Sample	RT			LT		
	M at 2 T (Am^2kg^{-1})	M_r (Am^2kg^{-1})	H_c (kA/m)	M at 5 T (Am^2kg^{-1})	M_r (Am^2kg^{-1})	H_c (kA/m)
Mt	0.057	0.003	2.440	6.554	0.017	3.065
MMt	1.695	0.004	0.018	9.116	0.790	26.502
Ver	0.275	0.004	0.945	14.383	0.031	2.378
MVer	1.113	0.146	6.066	13.912	0.414	18.503

component obtained by analysis of the Mössbauer spectrum at RT and more outstanding at the 7 K spectrum. A positive contribution to good magnetic parameters is also a visibly smaller particle size as it follows from TEM in Figure 6 (right panel bottom). It is supported by a well-known dependence of coercivity on the grain size presented by Herzer in [50]. Moreover, the particles in MMt are not agglomerated as it is at modified vermiculite, and therefore, the MVer sample embodies higher coercivity and remnant magnetization. The influence of particle agglomeration refer to the prevailing contributions of anisotropic energy reducing the magnetization at 1.6 MA/m (2 T) compared to the MMt sample.

The interparticle magnetic interactions were analyzed by Henkel plots using (1). While the original samples behave practically as noninteracting systems with very low negative magnetic dipole interactions (not presented), several times stronger interactions are observed for magnetically modified samples (Figure 9(c)). Positive exchange interactions dominate in the MMt sample due to low distances among separated very small nanoparticles. Interaction maximum is detected at magnetic fields about 60–80 kA/m. Contrarily, in the modified vermiculite the large objects of the small but agglomerated particles contribute to a visibly higher distances among them. Consequently, the negative dipole

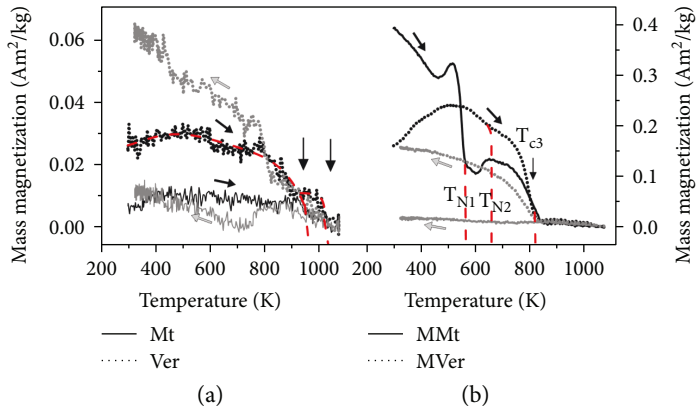

FIGURE 10: Thermomagnetic curves of the original (Ver, Mt) (a) and magnetically modified (MVer, MMt) samples (b) measured in an external magnetic field of 8 kA/m.

interactions with maximum at the lower magnetic field 11 kA/m prevail. It means that particles interact mainly through their total magnetic moments.

The thermomagnetic curves of samples in the original and magnetically modified states are presented in Figure 10. The measurements were done in an external magnetic field of 8 kA/m, and due to small magnetic moments of both samples in the original states (Ver, Mt), the curves are not smooth and the measurements reach a limit of equipment sensitivity. Magnetization curves at increasing temperature (Figure 10(a)) consist of two parts (red dashed lines), better resolved at the Ver sample. The first part decreases to zero at T_{C1}~950 K corresponding to the Curie temperature of the α-Fe_2O_3 phase [46] and the second one at T_{C2}~1040 K agrees with the Curie temperature of α-Fe.

The TMC curves in Figure 10(b) are visibly different due to the magnetic modification reflecting changes in Fe-based compounds. The Curie temperature T_{C3}~820 K for MVer and MMt samples corresponds to a ferromagnetic-paramagnetic transition of maghemite, γ-Fe_2O_3, [47] and thereby supports the Mössbauer results. The other two temperatures, Néel temperatures T_{N1} and T_{N2}, are very probably antiferromagnetic-paramagnetic transitions of the odd iron oxide and/or oxyhydroxide compounds.

The cooling of all samples back to room temperature returns them into a weak ferromagnetic and/or antiferromagnetic state with different magnetizations indicating the irreversible changes in the magnetic behaviour of powders treated up to 1073 K.

The behaviour of all samples below RT is documented by the FC/ZFC curves and hysteresis loops at 2 K shown in Figure 11 (Ver, Mt) and Figure 12 (MVer, MMt). The shape of FC/ZFC curves of Ver and Mt samples is practically identical showing slow changes of magnetization from 300 K to 25 K followed by its sharp increase from 25 K to 2 K. Such phenomenon was already observed, e.g., in hematite nanorods [51] or in CeO_2/α, γ-Fe_2O_3 nanocomposites [52], and could be ascribed to the magnetic phase transformation coming from ordering of surface spins at low temperatures and resulting in prevailing exchange interactions among iron oxide particles and increase of magnetization.

The LT loops of samples in both original and magnetically modified states document that their saturation is not achieved even in the applied external field of 5 T (4 MA/m). The main reason could be in the presence of metal and ionic compounds, in different influences of ferrous and/or ferric iron, in very small grains, and also in a direction of the applied field with regard to direction of the sheets [53]. All magnetic parameters determined from the LT loops of the original and magnetically modified samples yield higher values compared to RT parameters (see Table 4).

The ZFC curves for MVer and MMt samples differ. The ZFC curve of the MVer sample shows an atypical behaviour when it decreases nearly linearly with decreasing temperature and at about 25 K an inexpressive maximum denoted as blocking temperature T_B can be seen at this curve (inset in Figure 12—upper right panel). This T_B temperature separates the high-temperature superparamagnetic state from the low-temperature blocked state of magnetic moment of nanoparticles. Another characteristic value is irreversible temperature T_{irr} defining a point at which the ZFC and FC curves separate. It corresponds to blocking temperature of the largest nanoparticles in the system and achieves here 300 K. Minimum at the ZFC curve and subsequent increase in magnetization below about 10 K is related again to the surface spins of particles, effect observed already at original samples.

The magnetically modified montmorillonite (MMt) exhibits contrary to the MVer sample superparamagnetic behaviour at RT with nearly zero coercive field and remnant magnetization. It means that temperature fluctuations of nanoparticles easily overcome the barrier consisting of their anisotropic energy. However, marked increase of H_c up to 26.5 kA/m at 2 K confirms that during cooling of the MMt sample, magnetic nanoparticles attract the properties typical for magnetically ordered materials and pass into the blocking state at $T_B \approx 150$ K (see Figure 12).

The difference between blocking T_B (150 K) and irreversible T_{irr} (~200 K) temperatures is relatively small and reflects a narrow size distribution of particles. Moreover,

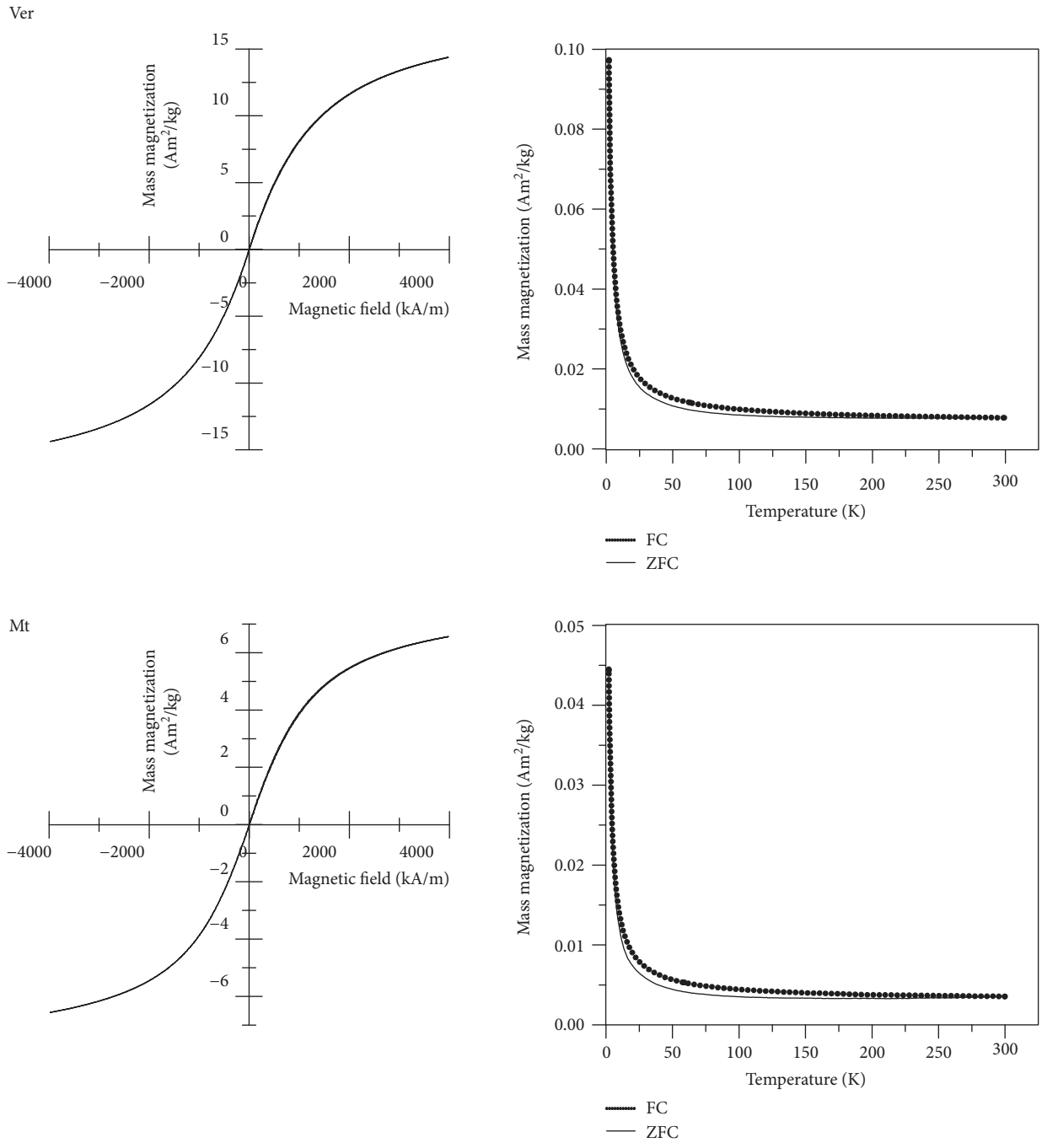

Figure 11: Low-temperature magnetization curves of original (Ver, Mt) samples measured at 2 K supplemented by the ZFC/FC curves.

the FC curve below T_B is nearly constant which is typical for the system yielding strong interparticle interactions. The ZFC curve below about 10 K increases in a similar way as was observed at all previous samples reflecting an influence of the spins.

4. Conclusions

Montmorillonite from the smectite group and vermiculite from the vermiculite group were magnetically modified by mixing the original clay minerals with iron oxide particles prepared using a microwave irradiation procedure. The complex structural and magnetic studies of the original and magnetically modified powders were performed using scanning and transmission electron microscopy, X-ray fluorescence spectroscopy, X-ray diffraction, Mössbauer spectrometry, and magnetic methods at room temperature. Most of the results is supported also by low-temperature measurements. Both clay minerals are of the 2 : 1 layer type, and SEM observations yield similar morphology and large-area as local-dot chemical homogeneity of all studied samples. Nevertheless, the TEM micrographs clearly show

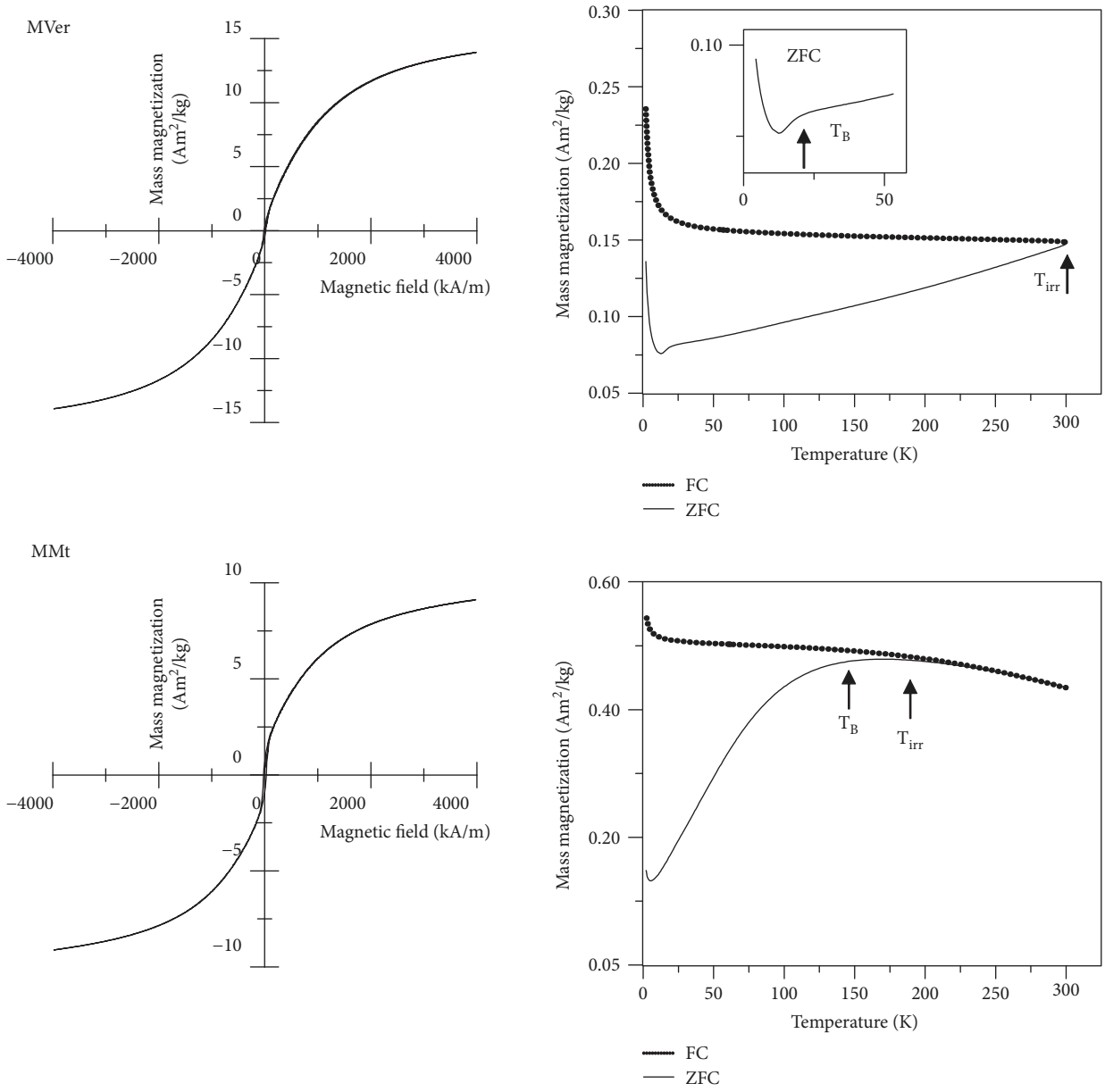

Figure 12: Low-temperature magnetic properties of magnetically modified (MVer, MMt) samples.

larger particle agglomerates at the vermiculite sample contrary to montmorillonite consisting of very small separated nanoparticles. The original clay minerals behave in a way corresponding to their composition; vermiculite with higher content of the iron-based compounds yields slightly softer magnetic properties and the presence of magnetic component at low temperature while montmorillonite is paramagnetic and/or superparamagnetic at both room and low temperatures. The magnetic modification changes the magnetic properties of both samples in different ways. The particle agglomerates in vermiculite cause magnetic hardening and prevailing dipolar interaction or dipolar coupling which refers to the direct magnetostatic interaction between two magnetic dipoles (moments). Contrary, the magnetically modified montmorillonite exhibits superparamagnetic behaviour at RT with nearly zero coercive field and remnant magnetization. It means that temperature fluctuations of nanoparticles easily overcome the barrier consisting of their anisotropic energy. Marked increase of H_c at 2 K confirms that during cooling, the magnetic nanoparticles attract the properties typical for magnetically ordered materials and pass into the blocking state at $T_B \approx 150$ K.

Data Availability

The experimental data used to support the findings of this study are included within the article.

Conflicts of Interest

The authors declare that they have no conflicts of interest.

Acknowledgments

This work was financially supported by the project SP2018/43 from ERDF/ESF New Composite Materials for Environmental Applications (No. CZ.02.1.01/0.0/0.0/17_048/0007399), by the CEITEC 2020 National Sustainability Programme II (No. LQ1601) and the project LO1305 both funded by Ministry of Education, Youth and Sports of the Czech Republic, by the Grant Agency of the Czech Republic (No. 13-13709S), and by the scientific researchers of higher education institutions within the State Task of the Russian Federation No. 2014/236.

References

[1] F. Bergaya, B. K. G. Theng, and G. Lagaly, Eds., *Handbook of Clay Science*, vol. 1, Elsevier, Developments of Clay Science, Amsterdam, Netherlands, 2006.

[2] T. B. Musso, K. E. Roehl, G. Pettinari, and J. M. Vallés, "Assessment of smectite-rich claystones from Northpatagonia for their use as liner materials in landfills," *Applied Clay Science*, vol. 48, no. 3, pp. 438–445, 2010.

[3] X. Zheng, J. Dou, J. Yuan, W. Qin, X. Hong, and A. Ding, "Removal of Cs^+ from water and soil by ammonium-pillared montmorillonite/Fe_3O_4 composite," *Journal of Environmental Sciences*, vol. 56, pp. 12–24, 2017.

[4] J. Wang, Y. Chen, G. Liu, and Y. Cao, "Synthesis, characterization and photocatalytic activity of inexpensive and non-toxic Fe_2O_3–Fe_3O_4 nano-composites supported by montmorillonite and modified by graphene," *Composites Part B: Engineering*, vol. 114, pp. 211–222, 2017.

[5] S. Mukherjee, *The Sciences of Clays—Applications in Industry, Engineering and Environment*, vol. 1, Capital Publishing Company and Springer, New Delhi, India, 2013.

[6] Z. Weiss and M. Kužvart, *Clay Minerals: Their Nanostructure and Utilization*, Karolinum, Prague, Czech Republic, 2005.

[7] J. Tokarsky, *Prepared Figures by Molecular Modelling Using Accelrys Materials Studio, (Software, unpublished)*, 2016.

[8] R. T. Martin, "Report of the clay minerals society nomenclature committee: revised classification of clay materials," *Clays and Clay Minerals*, vol. 39, no. 3, pp. 333–335, 1991.

[9] G. Lagaly, "Layer charge heterogeneity in vermiculites," *Clays and Clay Minerals*, vol. 30, no. 3, pp. 215–222, 1982.

[10] J. W. Gruner, "The structures of vermiculites and their collapse by dehydration," *American Mineralogist*, vol. 19, no. 12, pp. 557–575, 1934.

[11] H. Shirozu and S. W. Bailey, "Crystal structure of A2-layer Mg-vermiculite," *American Mineralogist*, vol. 51, pp. 1124–1143, 1966.

[12] J. Wang, G. Liu, C. Zhou, T. Li, and J. Liu, "Synthesis, characterization and aging study of kaolinite-supported zero-valent iron nanoparticles and its application for Ni(II) adsorption," *Materials Research Bulletin*, vol. 60, pp. 421–432, 2014.

[13] T. B. Musso, F. M. Francisca, G. Pettinari, and K. E. Roehl, "Suitability of a cretaceous natural Na-bentonite as construction material for landfill liners," *Environmental Engineering and Management Journal*, vol. 15, no. 11, pp. 2519–2528, 2016.

[14] T. S. Anirudhan, C. D. Bringle, and P. G. Radhakrishnan, "Heavy metal interactions with phosphatic clay: kinetic and equilibrium studies," *Chemical Engineering Journal*, vol. 200-202, pp. 149–157, 2012.

[15] T. B. Musso, M. E. Parolo, G. Pettinari, and F. M. Francisca, "Cu(II) and Zn(II) adsorption capacity of three different clay liner materials," *Journal of Environmental Management*, vol. 146, pp. 50–58, 2014.

[16] S. Shahmohammadi-Kalalagh, "Isotherm and kinetic studies on adsorption of Pb, Zn and Cu by kaolinite," *Journal of Environmental Sciences*, vol. 9, no. 2, pp. 243–255, 2011.

[17] H. Sis and T. Uysal, "Removal of heavy metal ions from aqueous medium using Kuluncak (Malatya) vermiculites and effect of precipitation on removal," *Applied Clay Science*, vol. 95, pp. 1–8, 2014.

[18] J. Zhao and M.-C. He, "Theoretical study of heavy metal Cd, Cu, Hg, and Ni(II) adsorption on the kaolinite(0 0 1) surface," *Applied Surface Science*, vol. 317, pp. 718–723, 2014.

[19] C. Blachier, L. Michot, I. Bihannic, O. Barres, A. Jacquet, and M. Mosquet, "Adsorption of polyamine on clay minerals," *Journal of Colloid and Interface Science*, vol. 336, no. 2, pp. 599–606, 2009.

[20] L. Zhang, L. Luo, and S. Zhang, "Adsorption of phenanthrene and 1,3-dinitrobenzene on cation-modified clay minerals," *Colloids and Surfaces A: Physicochemical and Engineering Aspects*, vol. 377, no. 1–3, pp. 278–283, 2011.

[21] R. Zhang, W. Yan, and C. Jing, "Mechanistic study of PFOS adsorption on kaolinite and montmorillonite," *Colloids and Surfaces A: Physicochemical and Engineering Aspects*, vol. 462, pp. 252–258, 2014.

[22] A. S. Elsherbiny, "Adsorption kinetics and mechanism of acid dye onto montmorillonite from aqueous solutions: stopped-flow measurements," *Applied Clay Science*, vol. 83-84, pp. 56–62, 2013.

[23] L. Guz, G. Curutchet, R. M. Torres Sanchez, and R. Candal, "Adsorption of crystal violet on montmorillonite (or iron modified montmorillonite) followed by degradation through Fenton or photo-Fenton type reactions," *Journal of Environmental Chemical Engineering*, vol. 2, no. 4, pp. 2344–2351, 2014.

[24] K. A. Selim, M. A. Youssef, F. H. Abd El-Rahiem, and M. S. Hassan, "Dye removal using some surface modified silicate minerals," *International Journal of Mining Science and Technology*, vol. 24, no. 2, pp. 183–189, 2014.

[25] M. T. Yagub, T. K. Sen, S. Afroze, and H. M. Ang, "Dye and its removal from aqueous solution by adsorption: a review," *Advances in Colloid and Interface Science*, vol. 209, pp. 172–184, 2014.

[26] J. L. Marco-Brown, M. M. Areco, R. M. Torres Sanchez, and M. dos Santos Afonso, "Adsorption of picloram herbicide on montmorillonite: kinetic and equilibrium studies," *Colloids and Surfaces A: Physicochemical and Engineering Aspects*, vol. 449, pp. 121–128, 2014.

[27] A. Parbhakar, J. Cuadros, M. A. Sephton, W. Dubbin, B. J. Coles, and D. Weiss, "Adsorption of L-lysine on montmorillonite," *Colloids and Surfaces A: Physicochemical and Engineering Aspects*, vol. 307, no. 1–3, pp. 142–149, 2007.

[28] W. Y. Hernandez, M. A. Centeno, J. A. Odriozola, S. Moreno, and R. Molina, "Acidity characterization of a titanium and sulfate modified vermiculite," *Materials Research Bulletin*, vol. 43, no. 7, pp. 1630–1640, 2008.

[29] H. Long, P. Wu, and N. Zhu, "Evaluation of Cs^+ removal from aqueous solution by adsorption on ethylamine-modified

montmorillonite," *Chemical Engineering Journal*, vol. 225, pp. 237–244, 2013.

[30] A. G. San Cristóbal, R. Castelló, M. A. Martín Luengo, and C. Vizcayno, "Acid activation of mechanically and thermally modified kaolins," *Materials Research Bulletin*, vol. 44, no. 11, pp. 2103–2111, 2009.

[31] S. Yang, M. Gao, Z. Luo, and Q. Yang, "The characterization of organo-montmorillonite modified with a novel aromatic-containing gemini surfactant and its comparative adsorption for 2-naphthol and phenol," *Chemical Engineering Journal*, vol. 268, pp. 125–134, 2015.

[32] L. Chen, C. H. Zhou, S. Fiore et al., "Functional magnetic nanoparticle/clay mineral nanocomposites: preparation, magnetism and versatile applications," *Applied Clay Science*, vol. 127-128, pp. 143–163, 2016.

[33] J. Yao, Y. Chen, H. Yu et al., "Efficient and fast removal of Pb(II) by facile prepared magnetic vermiculite from aqueous solution," *RSC Advances*, vol. 6, no. 103, pp. 101353–101360, 2016.

[34] A. P. M. Alves, M. G. Fonseca, and A. F. Wanderley, "Inorganic-organic hybrids originating from organosilane anchored onto leached vermiculite," *Materials Research*, vol. 16, no. 4, pp. 891–897, 2013.

[35] K. Pospiskova and I. Safarik, "Low-temperature magnetic modification of sensitive biological materials," *Materials Letters*, vol. 142, pp. 184–188, 2015.

[36] I. Safarik and M. Safarikova, "One-step magnetic modification of non-magnetic solid materials," *International Journal of Materials Research*, vol. 105, no. 1, pp. 104–107, 2014.

[37] D. Levy, R. Giustetto, and A. Hoser, "Structure of magnetite (Fe_3O_4) above the curie temperature: a cation ordering study," *Physics and Chemistry of Minerals*, vol. 39, no. 2, pp. 169–176, 2012.

[38] T. Zak and Y. Jiraskova, "CONFIT: Mössbauer spectra fitting program," *Surface and Interface Analysis*, vol. 38, no. 4, pp. 710–714, 2006.

[39] Y. Jiraskova, J. Bursik, O. Zivotsky, and J. Cuda, "Influence of Fe_2O_3 on alloying and magnetic properties of Fe–Al," *Materials Science and Engineering: B*, vol. 186, pp. 73–78, 2014.

[40] S. Thamm and J. Hesse, "A simple plot indicating interactions between single-domain particles," *Journal of Magnetism and Magnetic Materials*, vol. 154, no. 2, pp. 254–262, 1996.

[41] A. Argüelles, S. A. Khainakov, J. Rodríguez-Fernández, M. Leoni, J. A. Blanco, and C. Marcos, "Chemical and physical characterization of iron-intercalated vermiculite compounds," *Physics and Chemistry of Minerals*, vol. 38, no. 7, pp. 569–580, 2011.

[42] A. Campos, S. Moreno, and R. Molina, "Characterization of vermiculite by XRD and spectroscopic techniques," *Earth Sciences Research Journal*, vol. 13, no. 2, pp. 108–118, 2009.

[43] A. Wiewióra, J. L. Pérez-Rodríguez, L. A. Perez-Maqueda, and J. Drapala, "Particle size distribution in sonicated high- and low-charge vermiculites," *Applied Clay Science*, vol. 24, no. 1-2, pp. 51–58, 2003.

[44] A. Lerf, F. E. Wagner, and J. Poyato, "Mössbauer spectroscopic investigation of redox reactions in vermiculites from Santa Olalla (Huelva, Spain)," *Solid State Ionics*, vol. 141-142, pp. 479–486, 2001.

[45] J. M. D. Coey, "Mössbauer spectroscopy of silicate minerals," in *Mössbauer Spectroscopy Applied to Inorganic Chemistry*, G. J. Long, Ed., vol. 1 of Modern Inorganic Chemistry, pp. 443–509, Springer, Boston, MA, USA, 1984.

[46] F. E. Wagner and U. Wagner, "Mössbauer spectra of clays and ceramics," *Hyperfine Interactions*, vol. 154, no. 1–4, pp. 35–82, 2004.

[47] R. M. Cornel and U. Schwertmann, *Iron oxides—structure, properties, reactions, occurrences and uses*, WILEY-VCH Verlag, Weinheim, Germany, 2013.

[48] P. M. A. de Bakker, E. de Grave, R. E. Vandenberghe, and L. H. Bowen, "Mössbauer study of small-particle maghemite," *Hyperfine Interactions*, vol. 54, no. 1–4, pp. 493–498, 1990.

[49] R. Zboril, M. Mashlan, and D. Petridis, "Iron(III) oxides from thermal processes synthesis, structural and magnetic properties, Mössbauer spectroscopy characterization, and applications," *Chemistry of Materials*, vol. 14, no. 3, pp. 969–982, 2002.

[50] G. Herzer, "Nanocrystalline soft magnetic alloys," in *Handbook of Magnetic Materials*, K. H. J. Buschow, Ed., p. 4178, Elsevier Science B.V., 1997.

[51] Y. Zhao, C. W. Dunnill, Y. Zhu et al., "Low-temperature magnetic properties of hematite nanorods," *Chemistry of Materials*, vol. 19, no. 4, pp. 916–921, 2007.

[52] J. Luňáček, O. Životský, Y. Jirásková, J. Buršík, and P. Janoš, "Thermally stimulated iron oxide transformations and magnetic behaviour of cerium dioxide/iron oxide reactive sorbents," *Materials Characterization*, vol. 120, pp. 295–303, 2016.

[53] O. Ballet and J. M. D. Coey, "Magnetic properties of sheet silicates; 2 : 1 layer minerals," *Physics and Chemistry of Minerals*, vol. 8, no. 5, pp. 218–229, 1982.